Journal of Applied Electrochemistry **30**: 1119–1124, 2000.

Electrochemical and thermal behaviour of $LiNi_{0.8}Co_{0.2}O_2$ cathode in sealed 18650 Li-ion cells

W. LU, C.W. LEE, R. VENKATACHALAPATHY and J. PRAKASH*
Center for Electrochemical Science and Engineering, Department of Chemical and Environmental Engineering, Illinois Institute of Technology, Chicago, Illinois 60616, USA
*(*author for correspondence, e-mail: prakash@iit.edu)*

Received 24 November 1999; accepted in revised form 24 April 2000

Key words: accelerated rate calorimetry, area specific impedance, differential scanning calorimetry, Li-ion cell, $LiNi_{0.8}Co_{0.2}O_2$ cathodes

Abstract

The electrochemical performance of $LiNi_{0.8}Co_{0.2}O_2$ cathodes in Li ion cells was investigated under static and dynamic load conditions, which prevail in 'electric and hybrid vehicles' using 'constant current constant voltage and 'hybrid pulse power characteristic' procedures.The thermal properties of this cathode were investigated using the differential scanning calorimetric and accelerated rate calorimetric techniques. The cell fabricated with a $LiNi_{0.8}Co_{0.2}O_2$ cathode showed excellent power performance. The specific energy produced by the 18650 cell was 90 Wh kg^{-1} at 100 W kg^{-1} power level.

1. Introduction

Ambient lithium-ion rechargeable batteries based on the rocking chair concept are attractive for portable electronic devices as well as for electric vehicles (EVs) and hybrid vehicles (HVs) applications [1]. The important technical requirements of batteries and other energy sources for EVs and HVs are high specific energy and high power required during the dynamic load conditions. They require a wide range of electric power when driven in city traffic, which involves frequent changes in speed, braking, and while negotiating varied driving terrain. Therefore, it is important to understand the dynamic performance of cells under dynamic load conditions that prevail during the propulsion of EVs and HVs. The dynamic performance evaluation can be useful even at an early stage of cell R&D, when systems intended for EV propulsion are being evaluated. In HVs, several types of energy storage and conversion devices are combined to reduce the burden on one type of energy source. Mainly, for acceleration of the vehicle and other processes requiring high power to be discharged in short period of time, high power density devices such as electrochemical capacitors can be used. For driving a car (cruising etc.), high capacity energy sources can be used. Energy sources using Li ion chemistry are suitable for these applications. However, the issues related to operational reliability and thermal safety must be solved by changing cell chemistry and design. Typical cathode chemistries used for the Li ion cells are $LiCoO_2$, $LiNiO_2$, and $LiMn_2O_4$ [2–4]. $LiCoO_2$ was the first commercialized stable cathode material but its disadvantages are lower capacity and higher cost compared to $LiNiO_2$. The $LiNiO_2$ material, on the other hand, is thermally unstable and difficult to synthesize. $LiNi_{0.8}Co_{0.2}O_2$ cathodes can be hypothesized to have the merits of both $LiNiO_2$ and $LiCoO_2$ [5–7] materials and so may have improved capability to meet the performance requirements of EVs and HVs.

This paper presents the electrochemical and thermal behaviour of $LiNi_{0.8}Co_{0.2}O_2$ cathode material in Li ion cells under the operating conditions that prevail in EVs and HVs.

2. Experimental details

2.1. *Experiment set-up*

The 18650 Li ion cells containing $LiNi_{0.8}Co_{0.2}O_2$ cathode material were supplied by Argonne National Laboratory. The cells were built with a graphite anode, a $LiNi_{0.8}Co_{0.2}O_2$ cathode, a polypropylene separator, and a $LiPF_6$/EC-DMC (1:1) electrolyte. The average weight of the 18650 cells was about 39 g. The electrochemical performance was investigated using an Arbin cycler (ABTS 4.0) controlled by MIT 97 software in conjunction with a computer. The cells were cycled at room temperature.

2.2. *Static capacity and area specific impedance (ASI)*

Usually, the charge–discharge rate affects the static capacity due to the uncompensated resistance. The capacity measured during different constant current discharge is the criterion that determines the applicability of the cell in EVs and HVs. In these experiments, the constant current constant voltage (CCCV) technique was chosen for the charge process with an initial charge current of 0.2 A followed by trickle charging at 4.2 V. The delivered capacities at different discharge rates were calculated from the voltage–time curves.

The cell ASI values were measured by the current-interruption method. The cells were galvanostatically cycled at various rates. The current was interrupted intermittently for 30 s during discharge and the voltages were measured with time. The measured value of the voltage divided by the current density applied before the current interruption provided the ASI_t.

2.3. *Hybrid pulse power characterization (HPPC) study*

The HPPC profile was derived by the simplification of the real working process of the vehicle. The procedure is used [8] to characterize the performance of cell relative to the HV requirement. The HPPC profile shown in Figure 1 defines a dynamic current range instead of power for simple operation, which is characterized by various power levels associated with a typical driving pattern. The negative current in Figure 1 corresponds to discharge (driving) process, and the positive current corresponds to intermittent periods of charge (regenerative braking) process. To obtain the performance under different discharge states, the experiment was carried out at various depths of discharge (DOD). Initially, the cell was left on open circuit for a period of 1 h after 10% discharge at 1 *C* rate. The cell was then subjected to a pulse group (see Figure 1) comprising: (i) a 3 *C* discharge current pulse for 18 s; (ii) a rest period of 32 s followed by three regenerative pulses at 2.43 *C*, 1.89 *C* and 1.65 *C* rates for 2, 4 and 4 s duration, respectively;

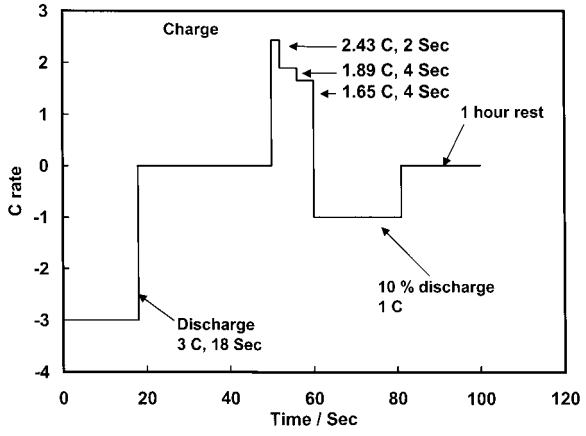

Fig. 1. Hybrid pulse power characterization profile for PNGV.

followed by (iii) a 10% discharge at a 1 *C*. The subsequent cycles were repeated after a 1 h rest period.

2.4. *Power performance and cycling efficiency during the HPPC*

To measure the electrochemical performance under different power discharges, the cell was subjected to constant power discharge from 20 to 640 W kg^{-1}. The coulombic efficiency of the cell was also determined during the cycling. One full cycle is described as a combination of charging the cell to 4.2 V, maintaining it at constant voltage until the current dropped to a value close to *C*/20, and then discharging the cell until its voltage reached 2.7 V. After every 10 cycles, the cell was routinely subjected to the HPPC profile.

2.5. *Differential scanning calorimetric (DSC) and accelerated rate calorimetric (ARC) methods*

The full size 18650 cell containing $LiNi_{0.8}Co_{0.2}O_2$ cathode was tested under thermal abuse conditions using the ARC–Arbin set-up. Within the temperature range of 30 °C–300 °C, the ARC was programmed in 'heat wait search' (HWS) mode to increase the temperature in steps of 10 °C, at a heating rate of 10 °C min^{-1}. ARC switches into the exothermic mode when the temperature gradient with time is found to be greater than 0.020 °C min^{-1}. Once an exothermic reaction is detected, the ARC follows it adiabatically and does not give any further step increase in temperature until the exothermic reaction has been completed. The details of the principle and operation of ARC are given elsewhere [9–12]. The change in the cell voltage with the increase in temperature was continuously monitored using an Arbin cycler (ABTS 4.0).

Differential scanning calorimetry (DSC 7, Perkin–Elmer) studies were conducted to investigate the thermal stability of graphite as anode and $LiNi_{0.8}Co_{0.2}O_2$ as cathode materials. $LiNi_{0.8}Co_{0.2}O_2$ and graphite were, for DSC studies, cycled to 4.2 V and 0.01 V respectively at the *C*/10 rate in 2016 half-cell. After cycling, the delithiated $LiNi_{0.8}Co_{0.2}O_2$ and the lithiated graphite in the cells were then recovered and sealed in standard aluminum DSC pans separately in a dry glove box. The DSC scans were carried out at a heating rate of 10 °C min^{-1}, from 30 to 300 °C under nitrogen purging.

3. Results and discussion

The discharge capacity of the Li-ion cell having $LiNi_{0.8}Co_{0.2}O_2$ cathode at various discharge rates is shown in Figure 2. The delivered capacity at a *C*/5 rate to 2.7 V cut-off voltage is 1.1 Ah. It can also be seen from this figure that the discharge capacity decreases as the discharge current increases. For instance, the cell produces only 0.9 Ah at a 1.2 *C* discharge rate. The lower capacity at higher discharge rate is related to

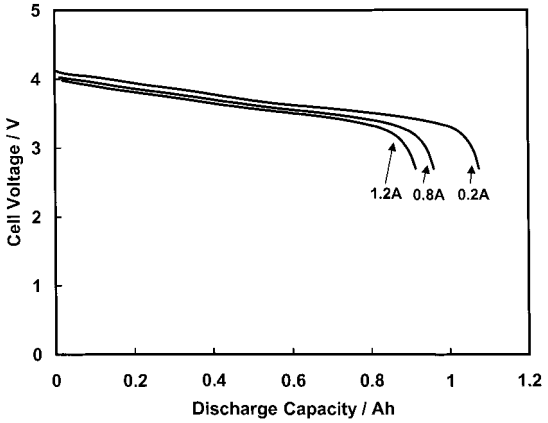

Fig. 2. Discharge curves of a 18650 cell fabricated with $LiNi_{0.8}Co_{0.2}O_2$ cathode at various discharge rates.

increased cell polarization due to changes in the Area Specific Impedance (ASI_t). The ASI_t, a parameter critically related to the entire cell performance, is time dependent and it includes the ohmic, electrolyte effects, and solid-state diffusion within the electrode. Impedance corresponding to certain interruption time is more useful and practical for EV and HV applications rather than complete relaxation to equilibrium after the interruption. The ASI_{30s} against DOD at 1.8 A and 0.8 A discharge currents are shown in Figure 3. The cell ASI_{30s} remains relatively constant up to 85% and then increases very sharply toward the end of discharge. The ASI_{30s} value of 2 *C* (1.8 A) discharge rate at the end of discharge is about 100 Ω cm^2. The 115 Ω cm^2 ASI_{15s} for *C*/1 discharge rate was given by Hong et al. [9] for cell containing $LiCoO_2$ cathode. A lower ASI_t value for the Li-ion cell containing $LiNi_{0.8}Co_{0.2}O_2$ cathode compared to the cell containing $LiCoO_2$ cathode is indicative of high energy and high power performance of the cell having $LiNi_{0.8}Co_{0.2}O_2$ cathode.

The typical voltage responses of 18650 cell to the HPPC profile (Figure 1) are shown in Figure 4(a). The ASI_t vs. DOD of 18 s interruption after 3 *C* discharge pulse and 2 s charge pulses calculated from Figure 4(a) are shown in Figure 4(b). The ASI_t of 18 s interruption

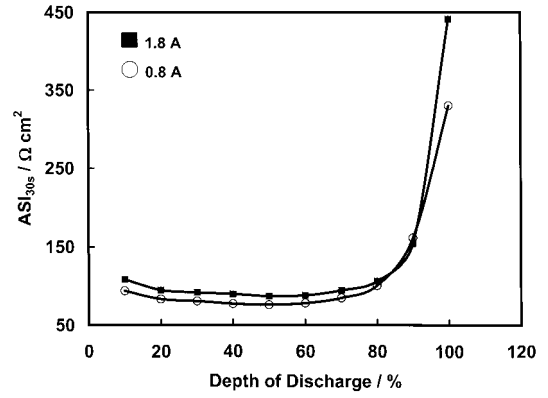

Fig. 3. Area specific impedance (ASI_{30s}) of a 18650 graphite/$LiNi_{0.8}Co_{0.2}O_2$ cell at various DOD.

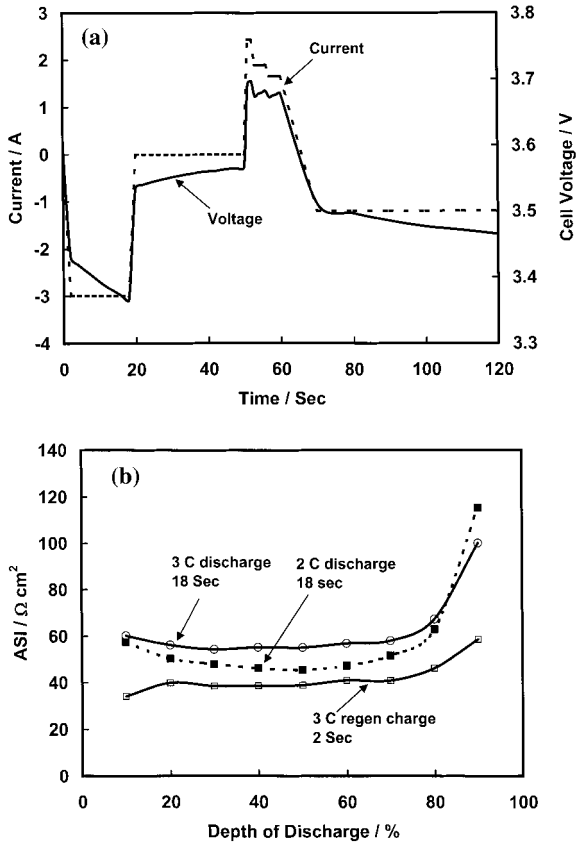

Fig. 4. 18650 cell: (a) Voltage response to HPPC profile shown in Figure 1; (b) ASI_t as function of DOD to HPPC profile containing $LiNi_{0.8}Co_{0.2}O_2$ cathode.

of 2 *C* discharge current is also shown in the Figure 4(b). As in constant current discharge (Figure 3), the cell ASI_t remains almost constant until the end of the discharge cycle. The cell impedance increases as the charge/discharge current pulse is increased. The ASI_{18s} of 3 *C* is 10% higher than that of 2 *C* discharge rate. A comparison of the HPPC ASI_t values (Figure 4(b)) and the constant current ASI_t (Figure 3) suggests that the current pulse discharge and constant current has same influence on the impedance.

Figure 5 shows the power performance of the 18650 cell at various discharge power levels. It can be seen form this figure that the discharge energy decreases with increasing discharge power levels. However, even at a power discharge level as high as 600 W kg^{-1}, the cell still produces a discharge energy of 50 Wh kg^{-1}. At a moderate power level of 200 W kg^{-1}, the cell produces about 90 Wh kg^{-1}. Based on these results, it can be concluded that a mid-size car using 300 kg battery system will achieve about 200 km range assuming 135 Wh km^{-1} consumption. This performance is consistent with the energy and power requirement of the EVs [13].

The change in coulombic efficiency as a function of repetitive cycling is shown in Figure 6. This figure shows that the cell produces superior performance in terms of coulombic efficiency. The efficiency is almost 100% for more than 60 cycles during the normal cycle. The

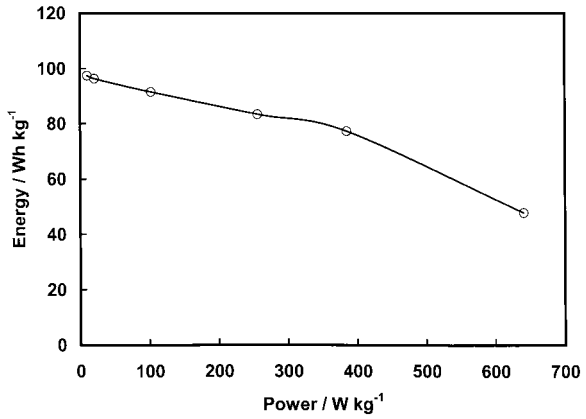

Fig. 5. Power performance of the 18650 cell containing $LiNi_{0.8}Co_{0.2}O_2$ cathode.

efficiency was found to be close to 96% even under HPPC testing conditions. The cell also showed an excellent capacity retention of about 96%.

Figure 7(a) and (b) show that the thermal behaviour of the electrolyte ($LiPF_6$ in EC/DMC) and a fully charged 18650 Li ion cell, respectively using ARC. It can be seen from Figure 7(a) that electrolyte alone does not show any detectable exothermic reaction in the temperature range of 30 to 250 °C. On the other hand, for fully charged Li ion cell the voltage drops to 0.0 V at about 165 °C suggesting internal cell shorting. This temperature indicates the onset temperature of thermal runaway in the Li ion cell. The self heat rate (SHR) profile calculated from the temperature profile (Figure 7(b)) is shown in Figure 7(c). Several exothermic peaks corresponding to various reactions are clearly visible in Figure 7(c). It is difficult to assign the exothermic peaks in Figure 7(c) to specific exothermic reactions involving anode or cathode. This is because ARC studies involved full cell comprising anode, cathode, electrolyte, binder, current collector, and nickel container. DSC studies, therefore, were carried out in order to understand the exothermic reactions corresponding to anode/electrolyte and cathode/electrolyte interface.

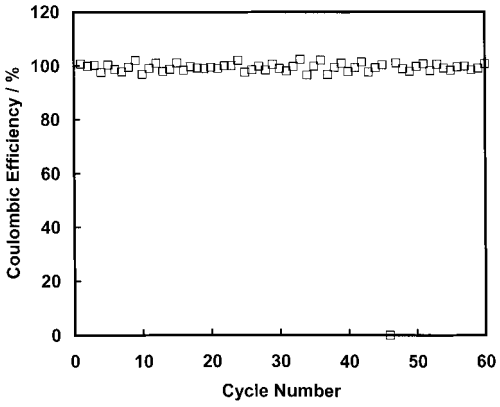

Fig. 6. Cycling efficiency of the 18650 cell containing $LiNi_{0.8}Co_{0.2}O_2$ cathode.

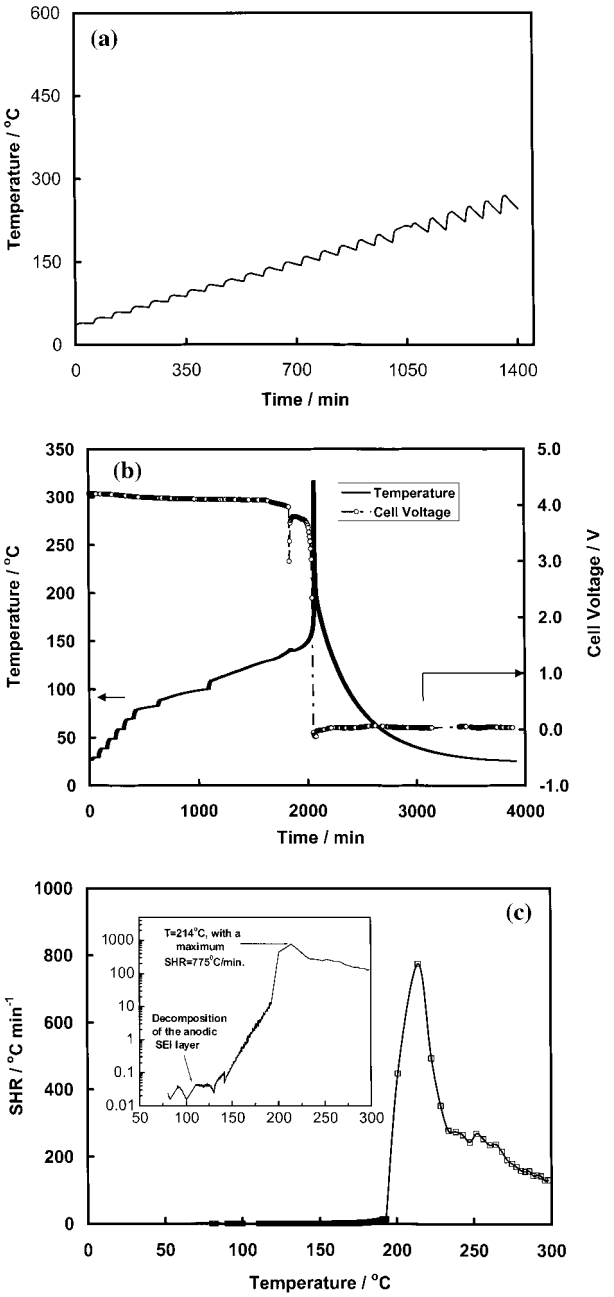

Fig. 7. Thermal considerations: (a) behaviour of Li-ion electrolyte ($LiPF_6$ in EC/DMC) using ARC; (b) runaway profiles of a fully charged 18650 Li ion cell using ARC; (c) self-heat rate profiles of electrolyte and 18650 cell under fully charged conditions. Inset shows log plot of SHR profiles.

Figure 8a and b show the DSC profiles of a delithiated $Li_xNi_{0.8}Co_{0.2}O_2$ cathode material and lithiated graphite anode material, respectively. It can be seen from Figure 8(a) that the exothermic reaction for delithiated $Li_xNi_{0.8}Co_{0.2}O_2$ cathode starts at about 168 °C with a major exothermic peak at 216 °C. On the other hand, the lithiated graphite anode shows an exothermic peak at about 120 °C followed by a major exothermic peak at 235 °C (Figure 8(b)). Based on these results, the exothermic peaks in the vicinity of 100 °C in Figure 7(c) can be attributed to the decomposition of

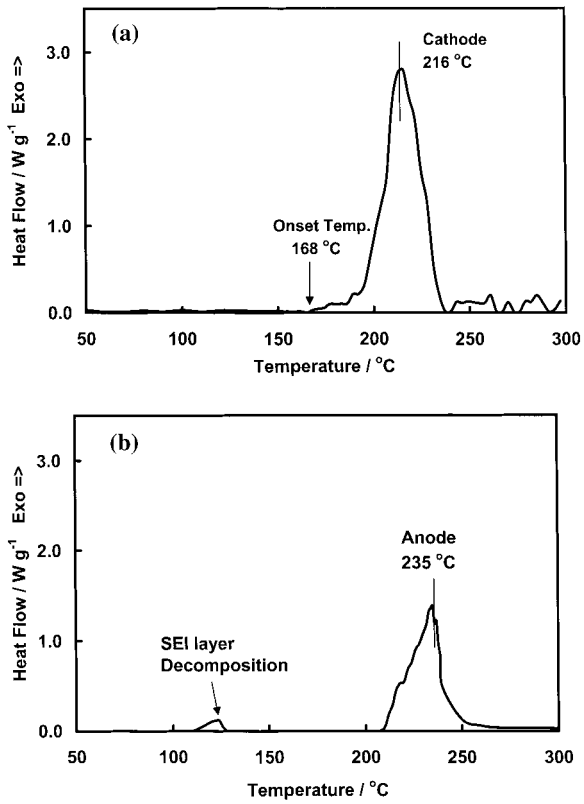

Fig. 8. DSC study: (a) $LiNi_{0.8}Co_{0.2}O_2$ cathode under fully charged conditions; (b) lithiated graphite anode.

the SEI layer formed on the anode surface, which is consistent with the studies carried out on similar materials [14]. In addition, The heat associated with the major exothermic peak from 165 to 235 °C (Figure 7(c)) is caused by the reactions of cathode/electrolyte and anode/electrolyte. The ΔH values for the cathode and anode, from DSC studies, were found to be 641 J g^{-1} and 317 J g^{-1}, respectively. From Figure 8(b), the net heat that could be generated, when 2.2 g of active anode material reacts with the electrolyte in the same temperature range, is 348 J. Similarly, the net heat that could be generated, when 5.87 g of active cathode material reacts with the electrolyte, is 3762 J from Figure 8(a). Thus, the total heat associated with the reactions of cathode–electrolyte and anode–electrolyte was calculated to be about 4110 J. On the other hand, the net heat generated for the exothermic peak occurring from 165 to 235 °C in ARC studies (Figure 7(c)) was found to be 3744 J, which is the same magnitude as calculated from DSC results. These results suggest that the major part of the exothermic peak in the temperature range of 168 to 230 °C at 214 °C (Figure 7(c)) is associated with the cathode–electrolyte reaction. However, the contribution of the graphite anode/electrolyte reaction to this exothermic reaction peak can not be completely neglected.

The heat and the temperature effects observed in the case of full cells tested in the ARC are an integral sum of the contributions from the individual components. To estimate the contribution from the individual components, the energy balance given by Bernardi et al. [15] is used:

$$Q = h_s(T - T_s) + MC_p\Delta T$$

where h_s is the heat transfer coefficient, T is the cell temperature, T_s is the surrounding temperature, M is the weight of the 18650 cell, ΔT is the difference between the onset of thermal runaway temperature (165 °C) and the temperature (230 °C) at which the major exothermic reaction ends. The heat stored in each component is calculated from their C_p values reported in Table 1. The C_p value for $LiNi_{0.8}Co_{0.2}O_2$ is estimated to be 1.23 J^{-1} g K^{-1} based on the C_p value for the $LiCoO_2$ [13] and $LiNiO_2$ [16]. In addition, the C_p value for the nickel oxides is typically slightly larger than that of cobalt oxides [17]. Based on the C_p values of the individual components, the total heat retained in the 18650 cell is 1901 J. Hence, the net heat transferred to the surroundings was found to be 1842.7 J. The values of heat dissipation and heat retained in the cell suggest the requirement of a good thermal management system before the cell can be effectively applied to EVs and HVs.

4. Conclusions

Li ion cells fabricated with $LiNi_{0.8}Co_{0.2}O_2$ cathodes showed excellent energy and power performance under CCCV and HPPC testing protocols producing up to 90 Wh kg^{-1} specific energy at 100 W kg^{-1} discharge power level. ARC and DSC studies showed that the fully charged $LiNi_{0.8}Co_{0.2}O_2$ cathode material is stable up to 165 °C. The high energy and power performance characteristics of $LiNi_{0.8}Co_{0.2}O_2$ suggests its viability as the cathode material for Li ion batteries for high power applications. It was also concluded that the major part of the exothermic peak in the temperature range of 168 to 230 °C at 214 °C (Figure 7(c)) is associated with the cathode/electrolyte reaction. However, the contribution of the graphite anode/electrolyte reaction to this exothermic reaction peak cannot be completely neglected.

Table 1. C_p values and the net heat retained in each component of Li-ion cell

Material	Weight/g	C_p J^{-1} g K^{-1}	Ref: for C_p	$M\,C_p\Delta T$/J
Graphite	2.2176	1.184	13	175.9
$LiNi_{0.8}Co_{0.2}O_2$	5.8748	1.230	*	484.2
Separator (PP)	1.970	2.066	13	272.7
Aluminum (CC)	2.28	0.900	13	137.5
Copper(CC)	5.648	0.385	13	145.7
PVDF(Binder)	0.764	0.903	14	46.2
Ni container	20.25	0.471	16	639.1
Net heat stored				1901.3

* Estimated value based the heat capacities of $LiCoO_2$ [13], nickel oxide [16] and cobalt oxide [16]

Acknowledgements

This work was supported by the Chemical Technology Division of the Argonne National Laboratory. The authors are grateful to Dr Khalil Amine, and Mr Gary Henriksen of the Chemical Technology Division, Argonne National Laboratory for encouragement and support. The authors would like to thank Dr V.S. Donepudi, Department of Chemical and Environmental Engineering, Illinois Institute of Technology, for reviewing manuscript and technical comments.

References

1. D. Aurbach, M.D. Levi, E. Levi, B. Markovsky, G. Salitre and H. Teller, Proceedings on 'Batteries for Portable Applications and Electric Vehicles', Electrochemical Society, Pennington, NJ **97-18** (1997), p. 451.
2. J.R. Dahn, A.K. Sleigh, Hang Shi, J.N. Reimeers, Q. Zhang and B.M. Way, *Electrochim. Acta* **38** (1993) 1179.
3. A. Du Pasquier, A. Blyr, P. Courjal, D. Larcher, G. Amatucci, B. Gerand and J-M. Tarascon, *J. Electrochem. Soc.* **146** (1999) 428.
4. H. Huang, C.A. Vincent and P.G. Bruce, *J. Electrochem. Soc.* **146** (1999) 481.
5. C. Delmas, I. Sasdoune and A. Rougier, *J. Power Sources* **44** (1993) 595.
6. T. Ohzuku, A. Ueda, M. Nagayama, Y. Iwakoshi and H. Komori, *Electrochim. Acta* **38** (1993) 1159.
7. S. Yamada, M. Fujiwara and M. Kanda, *J. Power Sources* **54** (1995) 209–213.
8. Idaho National Engineering Laboratory, PNGV Cell Test Manual, Revision 1, DOE/ID-10597 (1998).
9. J.-S. Hong, H. Maleki, S. Al Hallaj, L. Redey and J.R. Selman, *J. Electrochem. Soc.* **145** (1998) 1489.
10. H. Maleki, S. Al Hallaj, J.R. Selman, R.B. Dinwiddie and H. Wang, *J. Electrochem. Soc.* **146** (1999) 947.
11. M. Hasegawa and Y. Arakawa, *J. Power Sources* **44** (1993) 523–529.
12. S.C. Narang, S.C. Ventura, B.J. Dougherty, M. Zhao, S. Smedley and G. Koolpe, US Patent, 5 830 600 (3 Nov. 1998).
13. M. Broussely, J.P. Planchat, G. Rigobert, D. Virey and G. Sarre, *J. Power Sources* **68** (1997) 8–12.
14. A. Du Pasquier, F. Disma, T. Bowmer, A.S. Gozdz, G. Amatucci and J.-M. Tarascon, *J. Electrochem. Soc.* **145** (1998) 472.
15. D. Bernardi, E. Pawlikowski and J. Newman, *J. Electrochem. Soc.* **132** (1985) 5.
16. Z. Zhang, D. Fouchard and J.R. Rea, *J. Power Sources* **70** (1998) 16.
17. Accelerating Rate Calorimeter (ARC) Instruction Manual, P/N 851-9001, Authur D Little, MA (1990) 4-2 to 4-53.